The final assembly of trehalose polyphleates takes place within the outer layer of the mycobacterial cell envelope

Laurie Thouvenel, Gautier Prevot, Laura Chiaradia, Julien Parra, Emmanuelle Mouton-Barbosa, Marie Locard-Paulet, Julien Marcoux, Maryelle Tropis, Odile Burlet-Schiltz, Mamadou Daffé, et al.

JBC ARTICLE

The final assembly of trehalose polyphleates takes place within the outer layer of the mycobacterial cell envelope

Received for publication, March 11, 2020, and in revised form, June 11, 2020 Published, Papers in Press, June 17, 2020, DOI 10.1074/jbc.RA120.013299

Laurie Thouvenel[1], Gautier Prevot[1], Laura Chiaradia[1], Julien Parra[1], Emmanuelle Mouton-Barbosa[1], Marie Locard-Paulet[1,2], Julien Marcoux[1], Maryelle Tropis[1], Odile Burlet-Schiltz[1], Mamadou Daffé[1], Christophe Guilhot[1], Gilles Etienne[1], and Christian Chalut[1,*]

From the [1]Institut de Pharmacologie et de Biologie Structurale, Université de Toulouse, CNRS, UPS, Toulouse, France and the [2]Novo Nordisk Foundation Center for Protein Research, University of Copenhagen, Copenhagen, Denmark

Edited by Chris Whitfield

Trehalose polyphleates (TPP) are high-molecular-weight, surface-exposed glycolipids present in a broad range of nontuberculous mycobacteria. These compounds consist of a trehalose core bearing polyunsaturated fatty acyl substituents (called phleic acids) and a straight-chain fatty acid residue and share a common basic structure with trehalose-based glycolipids produced by *Mycobacterium tuberculosis*. TPP production starts in the cytosol with the formation of a diacyltrehalose intermediate. An acyltransferase, called PE, subsequently catalyzes the transfer of phleic acids onto diacyltrehalose to form TPP, and an MmpL transporter promotes the export of TPP or its precursor across the plasma membrane. PE is predicted to be an anchored membrane protein, but its topological organization is unknown, raising questions about the subcellular localization of the final stage of TPP biosynthesis and the chemical nature of the substrates that are translocated by the MmpL transporter. Here, using genetic, biochemical, and proteomic approaches, we established that PE of *Mycobacterium smegmatis* is exported to the cell envelope following cleavage of its signal peptide and that this process is required for TPP biosynthesis, indicating that the last step of TPP formation occurs in the outer layers of the mycobacterial cell envelope. These results provide detailed insights into the molecular mechanisms controlling TPP formation and transport to the cell surface, enabling us to propose an updated model of the TPP biosynthetic pathway. Because the molecular mechanisms of glycolipid production are conserved among mycobacteria, these findings obtained with PE from *M. smegmatis* may offer clues to glycolipid formation in *M. tuberculosis*.

Mycobacteria are endowed with an unusually thick lipid-rich cell envelope. This structure contains several families of trehalose-containing glycolipids that interact with mycolic acids attached to the arabinogalactan to form an atypical outer membrane called the mycomembrane (1). Among these, the ubiquitous trehalose monomycolates and trehalose dimycolates are essential for viability (2). This group also includes species-specific glycolipids, such as di- and polyacyltrehaloses (DAT and PAT) and sulfolipids (SL), which are restricted to the human pathogen *Mycobacterium tuberculosis*, or lipooligosacharides that have been isolated from diverse fast- and slow-growing mycobacteria (1). Recently, we reported that trehalose polyphleates (TPP), a family of surface-exposed glycolipids originally described in *Mycobacterium phlei*, are widely distributed across mycobacterial species, including *Mycobacterium smegmatis* and the opportunistic pathogens *Mycobacterium abscessus* and *Mycobacterium avium* (3–5). TPP consist of octoacylated trehalose bearing seven C36:5 and C40:6 polyunsaturated fatty acids called phleic acids and a C14–C19 fatty acid residue. They share a common basic structure with SL and PAT from *M. tuberculosis* (6). The biological function of TPP in mycobacteria remains enigmatic. A recent study showed that TPP production in *M. abscessus* correlates with clump and cord formation, suggesting a potential role for these molecules in the virulence of this opportunistic human pathogen (7).

Formation and export of TPP involve at least four biosynthetic enzymes and an MmpL transporter, namely MmpL10, that are encoded by genes clustered at the TPP locus (5). These proteins display sequence similarities with enzymes required for SL and PAT production, indicating that the TPP pathway can serve as an informative model to describe glycolipid production in *M. tuberculosis*. Biosynthesis of TPP begins in the cytoplasm with the formation of a 2,3-diacyltrehalose intermediate bearing a C14–C19 fatty acyl group and a phleic acyl substituent. The transacylase enzyme PE encoded by the *MSMEG_0412* gene (previously referred to as *MSMEI_0402*), subsequently catalyzes transesterification of phleic acids between diacyltrehalose precursors to generate TPP. Finally, MmpL10 is involved in the translocation of TPP or/and of TPP precursors across the plasma membrane (5, 8).

Despite this knowledge, the late stages of the TPP biosynthetic pathway and the relationship between biosynthesis and transport of these compounds to the cell envelope remain elusive. The PE protein is predicted to be a membrane-anchored protein harboring a putative N-terminal signal peptide and a C-terminal α/β-serine hydrolase domain, consistent with its proposed role as an acyltransferase in TPP assembly (Fig. 1) (9, 10). Interestingly, Chp1 and Chp2, two membrane-bound acyltransferases, respectively involved in SL and PAT production in *M. tuberculosis*, share overall domain organization with PE (Fig. 1). It has been proposed that these enzymes catalyze the last step of SL and PAT assembly by a mechanism that is tightly

This article contains supporting information.

* For correspondence: Christian Chalut, christian.chalut@ipbs.fr.
Present address for Gautier Prevot: Eligo Bioscience, Paris, France.
Present address for Laura Chiaradia: Centre Hospitalier Territorial Gaston-Bourret, New Caledonia.
Present address for Julien Parra: Evotec, Toulouse, France.

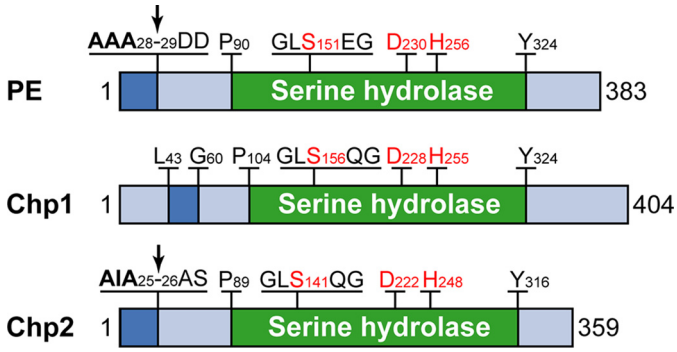

Figure 1. Domain organization of PE, Chp1, and Chp2. *In silico* analyses predict that PE (UniProtKB entry Q2M5K2, also referenced as "PE family protein" (UniProtKB entry I7FDB0)) and Chp2 (UniProtKB entry O50440) possess a putative N-terminal signal peptide (*dark blue boxes*) with an *AXA* signal peptidase cleavage motif (*boldface type*) (14), whereas Chp1 (UniProtKB entry O07801) contains a putative transmembrane helix (*dark blue box*) with no signal peptide cleavage site. Predicted cleavage sites in PE and Chp2 are indicated (*black arrows*). The three proteins harbor a conserved C-terminal domain (*green boxes*). Three-dimensional structure modeling of these domains revealed an α/β-hydrolase fold with an SDH catalytic triad (shown in *red*) and a conserved G*X*S*X*(G/S) pentapeptide motif sequence surrounding the serine residue, characteristic of serine hydrolase proteins (10). Predictions of transmembrane topology and signal peptides were performed using Phobius (RRID:SCR_015643) and SignalP 4.1 (RRID:SCR_015644).

coupled to lipid transport across the plasma membrane, but the molecular details of this process are not fully understood, partly because the *in vivo* subcellular localization of their catalytic domains remains controversial. Seeliger *et al.* (11) indeed demonstrated that the catalytic domain of Chp1 is located in the cytoplasm, but two studies reported contradictory results on the orientation of Chp2, the catalytic domain being either cytoplasmic or periplasmic (12, 13). Likewise, the orientation of PE in the plasma membrane and thereby the subcellular location of its catalytic domain, is unknown, raising questions on the cell compartment in which the transacylation step takes place and on the identity of the compounds that are transported by MmpL10.

The goal of this study was to shed light on the last step of TPP biosynthesis by investigating the topological organization and subcellular location of the PE protein. Using a combination of genetic, biochemical, and proteomic approaches, we established that PE has a C-terminal periplasmic domain and found that proteolytic cleavage of PE is required for efficient formation of TPP. Based on these data, we present here a refined model of the TPP biosynthesis pathway. This work provides clues for a better understanding of the molecular mechanisms involved in DAT/PAT production in *M. tuberculosis*.

Results

The C terminus of PE is located outside the plasma membrane

In silico analysis using the SignalP software predicts that PE possesses a putative signal sequence with a AXA signal peptidase I cleavage motif ($PE_{1\text{-}28}$, cleavage site between positions 28 and 29: AAA-DD, Fig. 1) (14); it is thus possible that this protein is associated with the plasma membrane, facing either the periplasm or the cytoplasm, or exported to the bacterial cell wall after cleavage of the signal sequence. To discriminate between these possibilities, we first investigated the topological organization of PE in *M. smegmatis*. Plasmids expressing PE fused at the C terminus with either the GFP or the alkaline phosphatase (PhoA) (Table S1) were introduced in the WT strain of *M. smegmatis*, and the GFP and PhoA activities were monitored to determine the subcellular localization of the reporter proteins. GFP exhibits fluorescence only when localized to the cytosolic compartment, whereas PhoA is only active inside the periplasmic space (15, 16). Expression of PE-GFP or PE-PhoA in an *M. smegmatis pE* knockout mutant (PMM229) restored TPP production, indicating that the fusion proteins are correctly folded and display proper subcellular localization in bacteria (Fig. S1). Additional *M. smegmatis* strains producing KatG1, a cytosolic protein, MmpL10, a transmembrane protein with a cytoplasmic C-terminal end, or MmpS4, a transmembrane protein with the C-terminal end facing the periplasm, fused to the same topology reporter proteins were generated to serve as controls in the experiments (16, 17). Bacteria producing PE-GFP displayed no increase in average fluorescence when compared with WT or control bacteria expressing MmpS4-GFP (Fig. 2*A*). Conversely, as expected, high fluorescence signals were detected for strains expressing KatG1-GFP or MmpL10-GFP. *M. smegmatis* strains producing the PhoA fusions were first assayed for alkaline phosphatase activity on LB agar plates containing the chromogenic substrate 5-bromo-4-chloro-3-indolyl phosphate (BCIP). Production of PE-PhoA resulted in blue colonies after incubation at 37 °C, indicative of PhoA activity (Fig. 2*B*). A similar pattern was observed for the control strain expressing MmpS4-PhoA, whereas no color change was observed for strains expressing either KatG1-PhoA or MmpL10-PhoA. To confirm these data, the PhoA activity of fusion proteins was assessed on cells grown in LB using the chromogenic substrate *p*-nitrophenylphosphate (pNPP). Results obtained were consistent with those obtained on BCIP agar plates: bacteria that express PE-PhoA, as well as those producing MmpS4-PhoA, exhibited high levels of PhoA activity compared with the WT strain and control strains expressing KatG1-PhoA or MmpL10-PhoA (Fig. 2*B*). Collectively, these data indicated that the C-terminal domain of PE is exposed on the outside of the plasma membrane. In these studies, we also sought to confirm the topology of Chp1 and to resolve the contradictory research findings regarding the topological organization of Chp2, using *M. smegmatis* strains expressing each of these proteins fused to either the GFP or PhoA. Attempts to detect GFP fluorescence or PhoA activity in bacteria producing the Chp1 fusion proteins failed (data not shown). For Chp2, we observed a significant PhoA activity in cells expressing Chp2-PhoA on both solid and liquid media, but no increase in fluorescence in bacteria producing Chp2-GFP, compared with the WT or the negative control MmpS4-GFP (Fig. 2, *A* and *B*), thus establishing that like PE, the Chp2 protein has its C-terminal domain exposed to the periplasmic space.

PE is present in the cell wall and secreted into the culture filtrate

Our topology studies revealed that the C-terminal domain of PE is located outside of the cytoplasm. To examine whether PE remains attached to the plasma membrane or is released into the bacterial cell wall, we performed a comprehensive

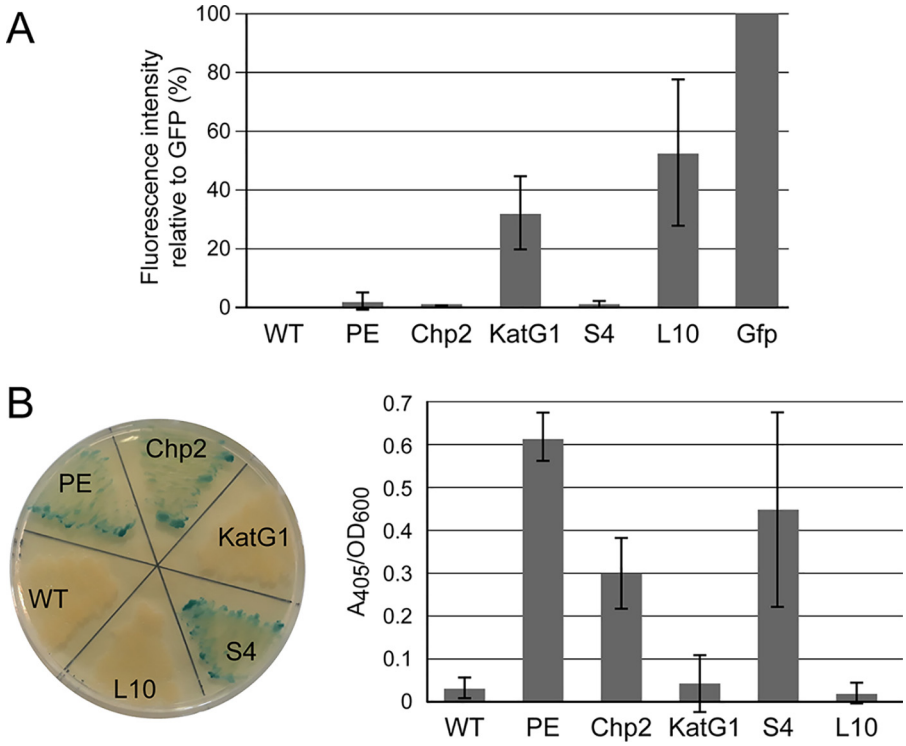

Figure 2. Subcellular localization of the C terminus of PE and Chp2. *A*, relative fluorescence intensities of *M. smegmatis* WT and of strains expressing PE, Chp2, KatG1, MmpS4 (S4), or MmpL10 (L10) tagged with the GFP protein at their C termini. Fluorescence intensity values were normalized to the OD_{600} of the cultures and were background-corrected by subtracting the fluorescence values of *M. smegmatis* WT. Data are expressed as percentages derived from the mean fluorescence intensity of each strain divided by the mean fluorescence intensity of an *M. smegmatis* strain expressing the GFP. Data shown on the graph are the average relative fluorescence values ± S.D. (*error bars*) measured in triplicate of three independent experiments. *B*, phosphatase alkaline activity of *M. smegmatis* WT and strains expressing PE, Chp2, KatG1, MmpS4 (S4), or MmpL10 (L10) fused to PhoA at their C termini. PhoA activities were tested on LB agar plates containing the chromogenic substrate BCIP (*left*). Blue colonies are indicative of PhoA activity. The PhoA activity was also evaluated on cells grown in LB using the chromogenic substrate pNPP (*right*). For each strain, the absorbance at 405 nm was normalized to the OD_{600} of the bacterial culture. Data shown on the graph are the average fluorescence values ± S.D. (*error bars*) measured in triplicate of three independent experiments.

proteomic analysis of the subcellular fractions of *M. smegmatis*. The proteomes of four independent cultures of *M. smegmatis* were split in four subcellular fractions: plasma membrane, culture filtrate (secretome), mycomembrane-containing cell-wall (MMCW), and soluble proteins from cytosol and periplasm. Plasma membrane and MMCW were isolated from the cell lysates by differential ultracentrifugation on a sucrose gradient, as described (18). The homogeneity of both membrane fractions has been demonstrated previously, using biochemical markers: arabinose and galactose (arabinogalactan), glucosamine, muramic acid, and diaminopimelic acid (peptidoglycan) as markers of MMCW and NADH oxidase and ATP synthase as markers of the plasma membrane. Only traces of MMCW markers were detected in the plasma membrane fraction, and conversely, very little NADH oxidase activity (3.6% of that measured in the plasma membrane) and no ATP synthase was detected in the MMCW fraction (18).

After concentration on SDS-PAGE, proteins from each fraction were digested in gel using trypsin. Peptides were then extracted from the gel and analyzed in quadruplicate injections by nano-LC–MS/MS using an Orbitrap Fusion™ Tribrid™ mass spectrometer. MS data were searched against the Uniprot *M. smegmatis* mc^2155 database for protein identification, and the quantitative comparison of relative protein abundances was performed using MS1-based label-free quantification. This data set contains 3,510 proteins and their relative quantities in the different fractions. We first confirmed the presence of proteins of known subcellular localization in the different fractions and their clustering based on MS signal (see Fig. S2 and Table S2 for the list of marker proteins). The PE protein was not detected in the cytosol or in the plasma membrane (Fig. 3*A*). It was detected with a very good sequence coverage in the MMCW (Fig. 3*B*). Although its signal was less intense, two specific peptides of PE were identified in the culture filtrate (see Fig. S3 for annotated spectra). Of note, the quantitative data relative to the subcellular specific proteomes generated in this study are available in Table S3. These data constitute an informative resource on the subcellular distribution of *M. smegmatis* proteins.

PE has a cleavable N-terminal signal sequence

As mentioned, PE possesses a putative signal sequence with a cleavage site. Therefore, we next examined whether the signal sequence is cleaved and whether the mature protein is exported to the MMCW using biochemical approaches. An HA-tagged PE protein (PE-HA) was expressed in the PMM229 mutant (Δ*pE*) of *M. smegmatis* for estimating its relative molecular weight in cells, based on SDS-PAGE migration and Western blotting analysis. Control strains producing either a mutated form of PE ($PE_{\Delta CS}$-HA), in which a stretch of amino acids (Ala^{26}–Asp^{29}) surrounding the putative cleavage site has been deleted to interfere with signal peptide removal, or the

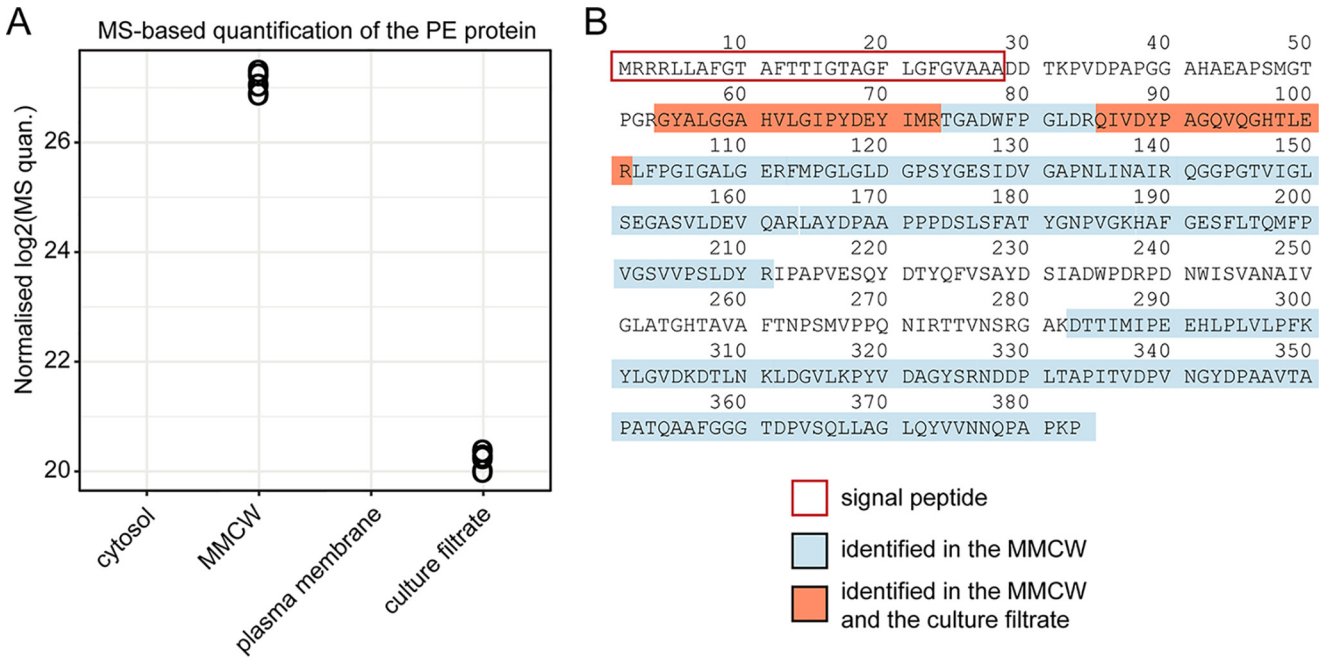

Figure 3. PE protein subcellular localization attested by quantitative proteomics. *A*, relative quantities of the protein PE (UniProtKB entry I7FDB0) in the four subcellular fractions (four biological replicates). *B*, sequence coverage of the PE protein in the MMCW and culture filtrate. The signal peptide located at PE N-terminal is indicated by a *red rectangle* (SignalP 5.0 prediction) (29).

predicted mature form of PE (mPE-HA, residues 29-383) were used to distinguish between cleaved and uncleaved forms of PE (Fig. 4*A*). Two protein bands that migrate at positions corresponding to mPE-HA and to the noncleavable $PE_{\Delta CS}$-HA variant, respectively, were detected in the cell extract of *M. smegmatis* expressing PE-HA, indicating that the PE protein underwent partial cleavage in this strain (Fig. 4*A*).

To further establish that PE contains a cleavable signal sequence, its N terminus region with or without the AAA motif and its local peptide environment was fused to the mature form of the *Escherichia coli* β-lactamase BlaTEM-1 (mBlaT, residues 24-286), generating fusion proteins PE_{1-25}-mBlaT and PE_{1-30}-mBlaT (Fig. 4*B*). BlaTEM-1 has been used before as a reporter for protein export with Sec and Tat substrates (19). PE_{1-30}-mBlaT and PE_{1-25}-mBlaT were expressed in PMM299, a *M. smegmatis* mutant lacking the major β-lactamase BlaS (see Fig. S4), and bacteria were tested for susceptibility toward ampicillin using a disk diffusion assay and the broth dilution method for MIC determination. Production of PE_{1-30}-mBlaT in PMM299 restored resistance to ampicillin beyond the WT level (more than 64-fold and 2-fold increases in MIC relative to the PMM299 mutant and the parent strain, respectively). In contrast, production of PE_{1-25}-mBlaT conferred only moderate resistance to ampicillin on both solid and liquid media (2–4-fold increase in MIC compared with the PMM299 mutant) (Fig. 4*B*).

To confirm that the difference we observed between the two proteins reflected a real difference in protein cleavage, we performed Western blotting analysis with an anti-BlaTEM-1 antibody on cell lysates prepared from PMM299 expressing either PE_{1-30}-mBlaT or PE_{1-25}-mBlaT. We found that the two proteins were produced in similar quantities in bacteria (Fig. 4*C*). In accordance with their calculated molecular weights (CMW), PE_{1-25}-mBlaT (CMW 31.8 kDa) migrated as a single band protein with an apparent molecular mass slightly higher than that of the full-length β-lactamase BlaTEM-1 (CMW 31.6 kDa), confirming that the protein was not processed in PMM299 (Fig. 4*C*). By contrast, two bands of similar intensity were visible for PE_{1-30}-mBlaT. Their migration on SDS-PAGE was consistent with the CMW of the full-length unprocessed form of the protein (32.3 kDa) and of the mature form of BlaTEM-1 with an additional DDKL amino acid sequence (DDKL-mBlaT, 29.4 kDa) (Fig. 4*C*). It can thus be concluded that PE_{1-25}-mBlaT remains attached to the plasma membrane due to the lack of signal sequence cleavage, causing a moderate increase in antibiotic resistance, whereas PE_{1-30}-mBlaT undergoes proteolytic processing, leading to mBlaT excretion in the cell envelope and high-level ampicillin resistance. Consistently, expression of BlaTEM-1 proteins with an altered cleavage signal sequence in *E. coli* confers intermediate-level resistance to ampicillin compared with the WT form of BlaTEM-1 (20). Altogether, data obtained with the BlaTEM-1 reporter protein, in addition to those obtained with the HA-tagged fusion proteins, confirmed that PE is excreted in the periplasmic compartment or the MMCW of *M. smegmatis* following signal peptide cleavage.

Cleavage of PE is required for efficient production of TPP

We finally explored whether formation of TPP in *M. smegmatis* depends on proteolytic cleavage of PE. Strain PMM229 (Δ*pE*) expressing either PE-HA or $PE_{\Delta CS}$-HA (Fig. 4*A*), as well as the WT and the PMM229 mutant strains, were grown to mid-exponential phase. The cellular and surface-exposed lipid fractions were extracted from each strain and separated by TLC. As reported previously, disruption of *pE* impaired TPP production and resulted in accumulation of a relatively polar compound that corresponds to the diacyl trehalose precursor of TPP, in both the cellular and surface compartments (5) (Fig.

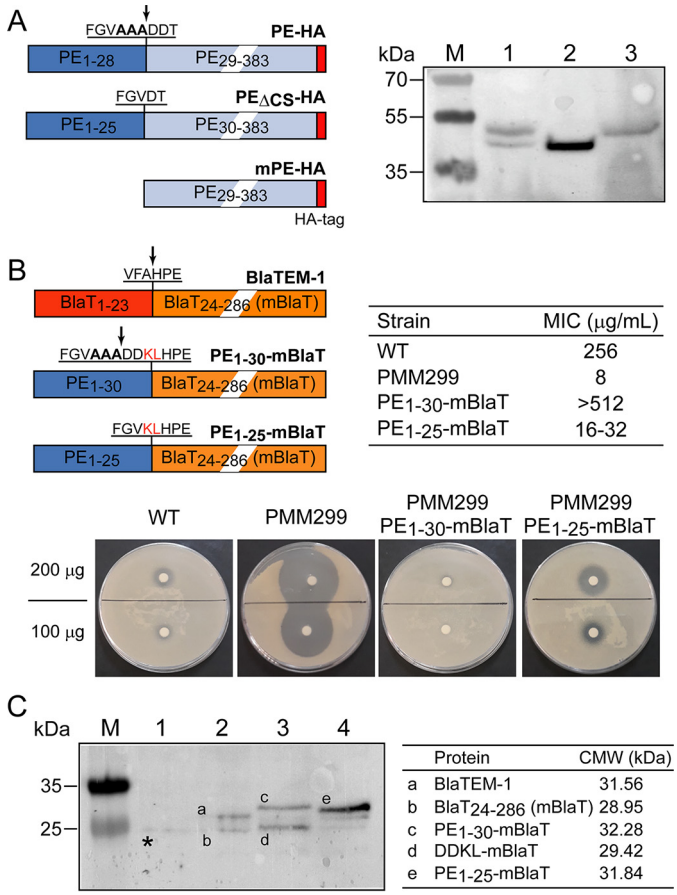

Figure 4. Cleavage of PE in *M. smegmatis*. *A*, Western blotting analysis of total cell lysates from PMM229 (Δ*pE*) expressing PE-HA (*lane 1*), mPE-HA (*lane 2*), or $PE_{\Delta CS}$-HA (*lane 3*), using an anti-HA antibody and an anti-mouse peroxidase conjugate (*right*). A schematic representation of the HA fusion proteins expressed in PMM229 is depicted on the *left*. The signal sequences of PE-HA and $PE_{\Delta CS}$-HA are represented by *dark blue boxes*, the region corresponding to the mature PE by a *light blue box* and the HA tag by a *red box*. The predicted cleavage site (*black arrow*) and amino acids encompassing the AAA signal peptidase cleavage motif (shown in *boldface type*) in PE-HA are indicated. *B*, ampicillin susceptibility of the WT and PMM299 (Δ*blaS*) mutant strains and of PMM299 expressing PE_{1-30}-mBlaT or PE_{1-25}-mBlaT. The MIC values of ampicillin obtained by the broth dilution method are shown in the *table*. The susceptibility to ampicillin was also evaluated by the disc diffusion method using disks containing 100 or 200 μg of ampicillin (*bottom*). A schematic representation of BlaTEM-1 and of PE-BlaTEM-1 fusion proteins is shown (*left*). The signal sequence and the mature form of BlaTEM-1 (mBlaT) are represented by *red* and *orange boxes*, respectively. Signal sequences of PE (PE_{1-28}/PE_{1-25}) fused to mBlaT are represented by *dark blue boxes*. Cleavage sites in BlaTEM-1 and PE_{1-30}-mBlaT are indicated by *arrows*. The amino acids encompassing the cleavage site in BlaTEM-1 and PE_{1-30}-mBlaT or the region connecting the transmembrane domain of PE and mBlaT in PE_{1-25}-mBlaT are indicated. *KL* in *red* corresponds to additional amino acids that were incorporated during the cloning process. *C*, Western blotting analysis of total cell lysates from the PMM299 mutant (*lane 1*) and from PMM299 expressing BlaTEM-1 (*lane 2*), PE_{1-30}-mBlaT (*lane 3*), or PE_{1-25}-mBlaT (*lane 4*), using an anti-BlaTEM-1 antibody and an anti-mouse peroxidase conjugate (*left panel*). Identities of protein bands detected by Western blotting (*labeled a–e*) and their CMW based on protein sequences are shown in the *table*. The *star* indicates a nonspecific band detected by the anti-BlaTEM-1 antibody in the PMM299 cell extract.

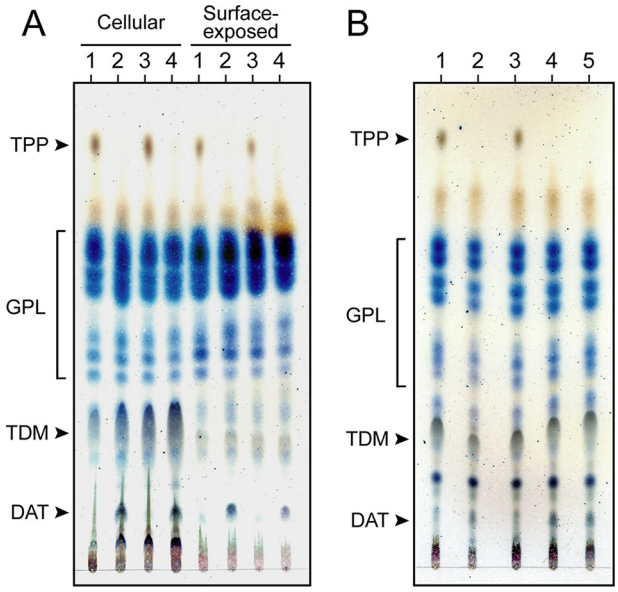

Figure 5. TPP production in PMM229 and in complemented strains expressing the HA-tagged PE variants, Chp1 or Chp2. *A* and *B*, cellular and surface-exposed lipid extracts from the WT strain (*lane 1*) and the PMM229 mutant strain (*lane 2*) and from the PMM229 strain expressing either PE-HA (*lane 3*) or $PE_{\Delta CS}$-HA (*lane 4*) (*A*) and total lipids extracted from the WT (*lane 1*) and PMM229 mutant (*lane 2*) strains and from the PMM229 strains expressing PE (*lane 3*), Chp1 (*lane 4*), or Chp2 (*lane 5*) (*B*) were loaded onto TLC plates run in $CHCl_3$/CH_3OH (90:10, v/v). The spots were visualized by spraying TLC plates with 0.2% (w/v) anthrone in concentrated H_2SO_4, followed by heating. Positions of TPP, diacyltrehalose TPP intermediates (DAT), GPL, and trehalose dimycolate (*TDM*) are indicated. Note that the absence of trehalose dimycolate in surface-exposed lipid fractions is consistent with previous reports and indicates that lipid fractions were properly prepared (30).

5*A*). Production of PE-HA in PMM229 restored the WT phenotype. In this complemented strain, TPP were found in the cellular and surface-exposed lipid fractions, and the intermediate product was undetectable in these lipid fractions. By contrast, PMM229 cells expressing the $PE_{\Delta CS}$-HA protein were defective in TPP production and accumulated the precursor in the cellular and surface compartments. These data demonstrate that the $PE_{\Delta CS}$-HA protein is unable to catalyze TPP formation, likely because the enzyme is anchored to the plasma membrane and has limited access to its substrate that is mainly located in the outer layers of the cell envelope. We cannot totally rule out that the small deletion present in $PE_{\Delta CS}$-HA may affect protein stability. However, amino acid residues surrounding the signal peptidase cleavage motif are located away from the predicted serine hydrolase core domain of PE (residues 90–324) and are probably not required for the correct folding of this domain. Supporting this, it has been shown that the Ala^{30}–Gly^{359} domain of Chp2, which starts 5 residues after the putative A*X*A cleavage motif (Fig. 1), displays acyltransferase activity *in vitro* (12).

Discussion

In a previous study, we proposed a model for the biosynthesis of TPP, but some steps of this biosynthetic pathway remain poorly characterized, including the one involving the acyltransferase PE (5). Here, we shed new light on the molecular mechanisms that underlie the latter stages of TPP production in *M. smegmatis*. Based on a series of genetic, biochemical, and proteomic approaches, we established that (i) the C-terminal domain of PE, and therefore its catalytic domain, resides outside the plasma membrane, (ii) PE is cleaved and excreted in the MMCW, and (iii) proteolytic processing of PE is required for efficient production of TPP in bacteria. These data, in

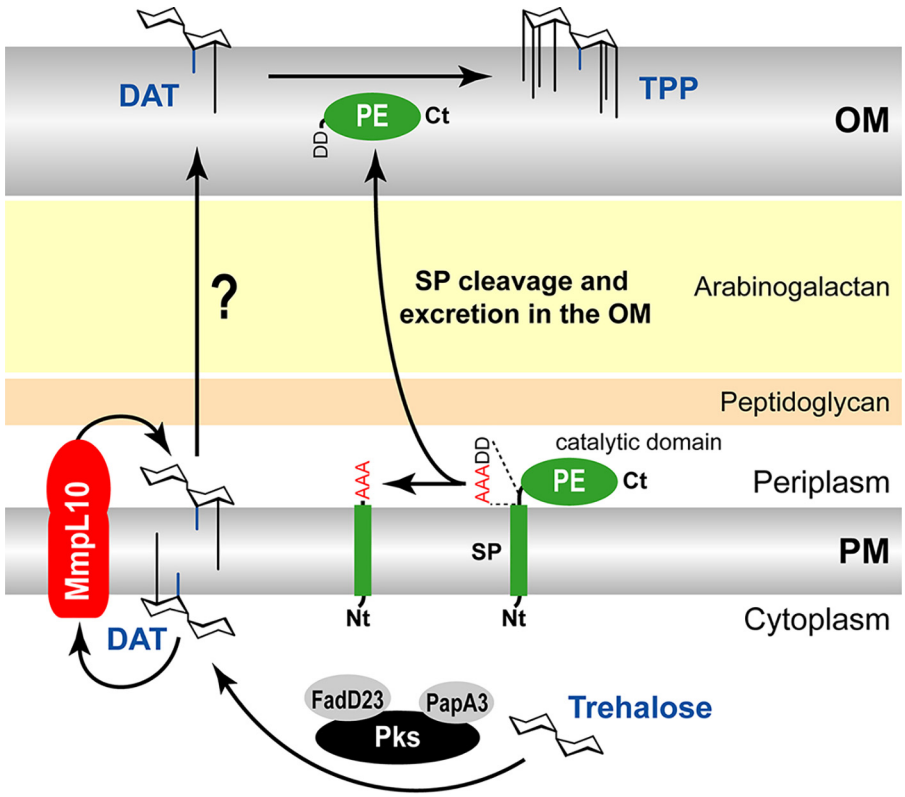

Figure 6. Update version of the late stages of the TPP metabolic pathway. Details are provided under "Discussion." C14–C19 fatty acyl groups and phleic acids present in the diacyltrehalose TPP intermediates (DAT) and TPP are represent by *blue* and *black lines*, respectively. *PM*, plasma membrane; *OM*, outer membrane (mycomembrane); *SP*, signal peptide; *Ct*, C terminus; *Nt*, N terminus. The AAA signal peptidase cleavage motif of PE is shown in *red*.

combination with our previous findings, allow us to propose an updated version of the TPP biosynthetic pathway (Fig. 6): the 2,3-diacyltrehalose precursor is synthetized through a series of cytoplasmic steps catalyzed by enzymes encoded by the TPP locus (FadD23, Pks, and PapA3) (5) and is translocated across the plasma membrane by the MmpL10 transporter. The intermediate molecule is then exported to the cell surface, where PE transacylates phleic acids between precursors to yield TPP. Several lines of evidence support this scenario. First, a *mmpL10* mutant of *M. smegmatis* is completely devoid of TPP, indicating that the transacylase reaction depends on the translocation process and likely occurs after this step (5). Second, accumulation of the intermediate product in the surface-exposed lipid fraction of the PMM229 (Δ*pE*) mutant indicates that this compound is translocated through the plasma membrane by MmpL10 and transferred to the cell surface. Third, we established that only the mature form of PE catalyzes TPP formation, supporting the notion that transacylation takes place in the cell envelope. Presumably, the full-length unprocessed PE protein is unable to perform this reaction because it has a restricted access to its substrate in the neighborhood of the plasma membrane.

In our Western blotting analyses, we observed partial cleavage of PE, likely due to a relative overexpression of the protein in the PMM229 mutant compared with the WT expression level. To visualize PE, we indeed used a PMM229 strain in which expression of *pE* was under the control of the strong promoter *pBlaF** (21) because we failed to detect protein production in cells carrying the *pE* gene under the control of its native promoter. Note that cleavage efficiency observed in our Western blotting experiments might be underestimated, due to a possible partial secretion of the processed form of PE, as evidenced by our proteomic studies. These studies, which identified PE in the MMCW but not in the plasma membrane of *M. smegmatis*, lend support to the idea that the protein exists primarily in a mature active form in the bacterium, when produced at physiological levels. BLAST searches in the GenBank™ database revealed that at least 100 mycobacterial species harbor the TPP locus and can potentially synthetize this family of glycolipids (Table S4). Interestingly, the presence of a predicted N-terminal signal sequence with a conserved A*X*A motif in the PE orthologs putatively produced by species containing the TPP locus indicates that secretion of these enzymes is a general process in TPP producers (Table S4).

The basic mechanisms underlying synthesis and export of trehalose-containing lipids are evolutionarily conserved in mycobacteria (8). Notably, it has been shown that two transmembrane acyltransferases, namely Chp1 and Chp2, sharing similar domain organization with PE, participate in SL and PAT assembly in *M. tuberculosis* by catalyzing sequential transesterification between SL precursors and DAT molecules, respectively. Despite similar functions in the formation of trehalose glycolipids, these acyltransferases exhibit strict substrate specificity because Chp1 and Chp2 are not functionally interchangeable for PAT and SL formation (13) and neither of the two enzymes can restore TPP production in the PMM229 mutant of *M. smegmatis* (Fig. 5*B*).

The C-terminal end of Chp1 was shown to reside in the cytosol, indicating that SL are built up intracellularly and exported to the cell envelope (11). The orientation of Chp2 in the plasma membrane is controversial because two studies demonstrated opposite orientation (12, 13). We were unable to confirm the topological organization of Chp1 using the reporter proteins GFP and PhoA in *M. smegmatis* because both Chp1-GFP and Chp1-PhoA were found to lack activity (data not shown). To demonstrate the cytosolic localization of the C-terminal domain of Chp1, Seeliger *et al.* (11) used the β-galactosidase reporter instead of the GFP. The absence of fluorescence with the Chp1-GFP fusion in our studies may result from protein misfolding. This hypothesis is nevertheless difficult to test experimentally in *M. smegmatis* because this bacterium does not produce SL and, as mentioned above, Chp1 cannot restore TPP production in a mutant strain lacking PE. Here, we provide evidence that the catalytic domain of Chp2 has a periplasmic localization when expressed in *M. smegmatis*. Although we failed to provide clear evidence that Chp2 is cleaved in this bacterium, the presence of an AXA motif at the end of the signal sequence strongly suggests that the protein might be converted to a mature form that is excreted in the periplasmic space in *M. tuberculosis*. In that situation, the scenario for DAT/PAT production would be similar to that of TPP in *M. smegmatis*: DAT would be synthesized in the cytosol and transferred to the bacterial cell surface to serve as a substrate for Chp2.

Despite significant progress made in understanding the mechanisms of glycolipid formation in mycobacteria, the molecular machinery involved in their transport across the cell envelope remains to be identified. For instance, it is not known whether MmpL10 cooperates with other proteins to promote TPP export. Using a GFP-trap pulldown approach, Fay *et al.* (22) recently identified two transmembrane proteins interacting with the MmpL3 transporter during mycolic acid transport in both *M. smegmatis* and *M. tuberculosis*, but no protein was found to bind MmpL10 in a parallel control experiment. Recent studies pointed out the role of lipoproteins in the export of several families of lipids in *M. tuberculosis*, but, to date, none of them has been shown to be involved in the transport of trehalose-containing glycolipids (23). The location of PE in the cell envelope makes this protein a suitable candidate as a bait for identifying interacting partners putatively involved in TPP transport. Delineation of the basic mechanisms that drive TPP transport in the mycobacterial model organism *M. smegmatis* may serve as a guide to describe export of glycolipids in *M. tuberculosis*.

Experimental procedures

Bacterial strains, growth media, and culture conditions

Plasmids were propagated at 37 °C in *E. coli* DH5α in LB broth or LB agar (Invitrogen) supplemented with either kanamycin (Km) (40 μg/ml) or hygromycin (Hyg) (200 μg/ml). *M. smegmatis* mc^2155 WT and derivatives (Table S5) were grown at 37 °C in LB broth or in Middlebrook 7H9 broth (DB Difco) containing ADC (0.2% dextrose, 0.5% BSA fraction V, 0.0003% beef catalase) and 0.05% Tween 80 when necessary and on LB agar. When required, Km and Hyg were used at a concentration of 40 and 50 μg/ml, respectively. For subcellular fractionation and MS analysis, *M. smegmatis* mc^2155 was grown in 7H9 Middlebrook broth medium supplemented with 0.2% glycerol (Sigma) at 37 °C with shaking at 180 rpm.

Construction of the M. smegmatis blaS-disrupted mutant

The *M. smegmatis blaS* mutant (PMM299) was constructed by homologous recombination using pWM290, a derivative of the mycobacterial suicide plasmid pJQ200 harboring the counterselectable marker *sacB* (24). Briefly, two DNA fragments encompassing the regions located upstream and downstream of the *blaS* gene (*MSMEG_2658*) (25) were amplified by PCR from *M. smegmatis* mc^2155 total DNA and inserted, flanking a *res-km-res* resistance cassette, into pWM290. The resulting plasmid (pWMbla) was transferred by electroporation into *M. smegmatis* mc^2155 for allelic exchange, and transformants were selected on plates containing Km and sucrose. Several Km- and sucrose-resistant colonies were screened by PCR with different primer combinations. For further details, see Fig. S4.

Construction of protein expression vectors

Plasmids used in this study are indicated in Table S1. Details of plasmid constructions are described in the supporting information.

Fluorescence and alkaline phosphatase-based assays for topology determination of PE

The subcellular location of the C-terminal region of PE was investigated using the topology reporter proteins PhoA and GFP (15, 16). To measure the fluorescence intensities of strains expressing the GFP fusion proteins, bacteria were grown in LB containing 0.05% Tween 80 to logarithmic phase. Bacterial concentrations were determined by OD_{600} measurements, and 500 μl of each culture were centrifuged for 1 min at 12,000 rpm. Pellets were resuspended in 500 μl of PBS containing 0.05% Tween 80, and 100 μl of each bacterial suspension were transferred to 96-well plates in triplicate. Fluorescence intensities were measured using a CLARIOstar microplate reader (BMG Labtech) at excitation and emission wavelengths of 470 and 515 nm, respectively. PhoA activities of *M. smegmatis* strains producing PhoA fusions were assessed by streaking bacteria on LB agar plates supplemented with 60 μg/ml BCIP. Plates were incubated at 37 °C for 4 days. PhoA activities were also measured on cells grown in liquid medium using the chromogenic substrate pNPP (New England Biolabs). Bacteria were cultivated in LB at 37 °C, and growth was followed by OD_{600} measurements. Bacteria were then washed twice with 1 M Tris, pH 8.0, containing 0.05% Tween 80, and the OD_{600} was adjusted to 2 with this buffer. 200 μl of cell suspension were mixed with 1 ml of buffer containing 10 mM pNPP and 10 mM $MgCl_2$ and incubated for 90 min at 37 °C in the dark. The reaction was stopped by adding 0.2 ml of 1 M K_2HPO_4 solution (Sigma). Tubes were centrifuged for 10 min at 13,000 rpm to remove aggregates, and 1 ml of supernatant was used to measure absorbance at 405 nm.

Antimicrobial susceptibility testing

Ampicillin susceptibilities of *M. smegmatis* strains expressing the BlaTEM fusion proteins were assessed using the disk diffusion method and by MIC measurements. For the disk diffusion assay, cultures were grown to mid-exponential phase (OD_{600} = 0.3–0.5) in 7H9 containing 0.05% Tween 80. Cells were washed once with fresh medium and resuspended in an equal volume of 7H9. 200 μl of cell suspension were mixed with 5 ml of molten top agar (0.6% agar, 0.2% glycerol (v/v)) and poured onto 7H11 plates supplemented with oleic acid/albumin/dextrose/catalase. Homemade discs containing 100 or 200 μg of ampicillin were placed on top, and plates were incubated for 3 days at 37 °C. MIC were determined by the broth microdilution method. Cultures were harvested at mid-exponential phase in 7H9 containing 0.05% Tween 80, and the OD_{600} values were adjusted to 0.3 with fresh medium. 10 μl of each culture were used to inoculate 1 ml of 7H9 supplemented with 0.05% Tween 80 containing 2-fold serially diluted ampicillin (from 512 to 1 μg/ml) in a 24-well plate (Nunc). Plates were incubated for 3 days at 37 °C with shaking at 150 rpm. The MIC corresponds to the lowest concentration of antibiotic inhibiting visible growth of bacteria.

Detection of proteins in bacteria by Western blotting analyses

To prepare whole-cell lysates of *M. smegmatis*, bacteria were grown in 50 ml of 7H9, collected by centrifugation, and resuspended in 500 μl of lysis buffer (20 mM Tris-HCl, pH 7.4). 500 μl of 0.1-mm glass beads (Biospec) were added to the cell suspensions, and bacteria were subjected to bead beating (Retsch Mixer Mill) for two cycles of 1 min with 2 min on ice between cycles. Tubes were centrifuged briefly to pellet beads and collect the supernatant fractions. Alternatively, 100–400 ml of bacterial cultures were collected and resuspended in 10 ml of lysis buffer. Cells were lysed by two passages through a French press, at 1,500 bars. For both methods, cell lysates were subjected to centrifugation at 3,000 × *g* for 10 min to remove nonlysed cells. To perform Western blotting analyses, proteins from whole-cell lysates were separated by SDS-PAGE and transferred onto nitrocellulose membranes (Pall Corp.). Membranes were incubated in 1 × PBS containing 0.1% Tween 20 and 10% nonfat dry milk and then incubated for 1 h with either a mouse monoclonal anti-HA antibody (clone HA-7, Sigma; 1:10,000) or a mouse monoclonal anti-BlaTEM-1 antibody (clone MA1-20370, Invitrogen; 1:400) in PBS containing 0.1% Tween 20 and 1% dry milk. Membranes were washed three times for 5 min with PBS containing 0.1% Tween 20 and incubated for 1 h with a horseradish peroxidase–conjugated goat anti-mouse IgG antibody (Sigma) at a dilution of 1:3,000 in PBS containing 0.1% Tween 20 and 1% nonfat dry milk. Protein bands were visualized using the EMD Millipore Immobilon enhanced chemiluminescence kit and a ChemiDoc Touch imaging system (Bio-Rad).

Extraction of mycobacterial lipids and TLC analyses

Bacteria were cultivated in LB medium at 37 °C and recovered by centrifugation (3,000 × *g*, 10 min). Total lipid fractions were extracted from bacterial pellets with chloroform/methanol (1:2) and chloroform/methanol (2:1), washed with water, and dried before analysis. Cellular and surface-exposed lipids were prepared as described previously (5, 26). Mycobacterial cell pellets were shaken for 1 min with 10 g of glass beads (4-mm diameter) per 2 g (wet weight) of cells and resuspended in distilled water. Extracellular materials were separated from cells by centrifugation (3,000 × *g*, 10 min). Cellular lipid fractions were then extracted from pellets with chloroform/methanol (1:2) and chloroform/methanol (2:1), washed with water, and dried before analysis. Surface-exposed lipids were extracted from supernatants with chloroform and methanol according to the Bligh and Dyer procedure (27). After drying, the organic phases were washed. For TLC analyses, equivalent amounts of lipids from each strain were spotted on silica gel G60 plates (20 × 20 cm; Merck) run in $CHCl_3/CH_3OH$ (90:10, v/v). The spots were visualized by spraying the plates with a 0.2% anthrone solution (w/v) in concentrated H_2SO_4, followed by heating.

Bacteria lysis and fractionation on sucrose density gradient for proteomics by MS

M. smegmatis cells were fractionated as described previously (18). Briefly, exponentially growing bacteria were harvested by centrifugation at 3,000 × *g* for 15 min at 4 °C. The supernatant was filtrated through a 0.2-μm sterile Nalgene filter to yield the culture filtrate, and proteins were concentrated using a 3,000-Da molecular weight cutoff Vivaspin. The pellet was suspended in lysis buffer (20 mM Tris-HCl, pH 7.4, containing 5 μl of benzonase nuclease >250 units/ml (Sigma–Aldrich), 1 mM DTT, 2 mM 4-(2-aminoethyl)benzenesulfonyl fluoride (Euromedex), and 1 mM EDTA), and bacterial cells were broken by two passages through a French press cell (1,500 bars). Unbroken bacteria were removed by centrifugation (3,000 × *g* for 10 min, twice). The bacterial lysate was then submitted to centrifugation at 10,000 × *g* for 40 min to yield a crude MMCW fraction (pellet P10) and S10 supernatant. P10 was suspended in 20 mM Tris-HCl, pH 7.4, containing EDTA (1 mM), layered on a sucrose step gradient (from 10% (w/w) to 60% (w/w)), and then centrifuged for at least 2 h at 100,000 × *g*. The MMCW fraction was recovered at the 30–36% sucrose cushion interface and washed twice with Tris-HCl buffer (10,000 × *g*, 1 h). The S10 supernatant was centrifuged at 27,000 × *g* for 30 min, and the resulting supernatant (S27) was further separated into supernatant (S100 fraction) and pellet (P100 fraction) by centrifugation at 100,000 × *g* for 40 min. S100 yielded the cytosolic fraction. The P100 was suspended in 20 mM Tris-HCl, pH 7.4, containing 1 mM EDTA before being layered on a sucrose step gradient (from 10% (w/w) to 60% (w/w)) and centrifuged for at least 2 h at 100,000 × *g*. Plasma membranes were recovered at the 20–30% sucrose cushion interface and washed twice with Tris-HCl buffer (100,000 × *g*, 1 h).

Protein digestion and nano-LC–MS/MS analysis

Subcellular fractions were analyzed on an Orbitrap Fusion™ Tribrid™ mass spectrometer (Thermo Fisher Scientific), as

described previously (18) but with slight modifications (see supporting information).

Bioinformatic MS data analysis

The Mascot (Mascot server version 2.6.2) database search engine was used for peptide and protein identification using automatic decoy database search to calculate a false discovery rate. MS/MS spectra were compared with the UniProt *M. smegmatis* strain ATCC700084/mc^{2}155 database (release June 2017, 12,683 sequences). See supporting information for more details about the data analysis.

Data availability

All the R scripts associated to this study are freely available with the Proline export tables on Zenodo (3686899). The MS proteomics data have been deposited to the ProteomeXchange Consortium via the PRIDE (28) partner repository with the data set identifier PXD017602.

Acknowledgments—We are grateful to Prof. Claude Gutierrez (IPBS, University of Toulouse) for providing the pPH07 plasmid.

Author contributions—L. T. and C. C. conceptualization; L. T., L. C., M. L.-P., J. M., G. E., and C. C. formal analysis; L. T., G. P., L. C., J. P., E. M.-B., M. L.-P., J. M., and C. C. investigation; L. T., G. P., L. C., J. P., E. M.-B., M. L.-P., J. M., and C. C. methodology; L. T., M. L.-P., J. M., O. B.-S., M. D., C. G., G. E., and C. C. writing-review and editing; M. L.-P. and J. M. data curation; M. L.-P., J. M., C. G., G. E., and C. C. writing-original draft; J. M. validation; M. T., O. B.-S., M. D., C. G., and C. C. funding acquisition; M. D. and C. C. supervision; C. C. project administration.

Funding and additional information—This work was supported by the Fondation pour la Recherche Médicale (FRM) Grant DEQ20160334879, CNRS, and the French Ministry of Research with the "Investissement d'Avenir, Infrastructures Nationales en Biologie et Santé" Program Grant ANR-10-INBS-08 (ProFI, Proteomics French Infrastructure project) (to O. B.-S.). L. T. is the recipient of a fellowship from the Ministry of Teaching and Scientific Research. M. L.-P. was supported by Novo Nordisk Foundation Grant NNF14CC0001. L. C. was a fellow of Province-Sud of New Caledonia.

Conflict of interest—The authors declare that they have no conflicts of interest with the contents of this article.

Abbreviations—The abbreviations used are: DAT, diacyltrehalose; BCIP, 5-bromo-4-chloro-3-indolyl phosphate; MMCW, mycomembrane-containing cell wall; pNPP, *p*-nitrophenylphosphate; PhoA, alkaline phosphatase; SL, sulfolipid(s); TPP, trehalose polyphleate(s); PAT, polyacyltrehalose(s); MIC, minimum inhibitory concentration; CMW, calculated molecular weight(s); LB, lysogeny broth; Km, kanamycin; Hyg, hygromycin; OD, optical density.

References

1. Daffe, M., Crick, D. C., and Jackson, M. (2014) Genetics of capsular polysaccharides and cell envelope (glyco)lipids. *Microbiol. Spectr.* **2,** MGM2-0021-2013 CrossRef Medline
2. Daffe, M., and Marrakchi, H. (2019) Unraveling the structure of the mycobacterial envelope. *Microbiol. Spectr.* **7,** GPP3-0027-2018 CrossRef Medline
3. Asselineau, C., Montrozier, H., and Promé, J. C. (1969) [Presence of polyunsaturated acids in bacteria: isolation of hexatriacontapentaene-4,8,12,16,20-oic acid and acid analogs from *Mycobacterium phlei* lipids]. *Eur. J. Biochem.* **10,** 580–584 CrossRef Medline
4. Asselineau, C. P., Montrozier, H. L., Promé, J. C., Savagnac, A. M., and Welby, M. (1972) [Polyunsaturated glycolipids synthesized by *Mycobacterium phlei*]. *Eur. J. Biochem.* **28,** 102–109 CrossRef Medline
5. Burbaud, S., Laval, F., Lemassu, A., Daffé, M., Guilhot, C., and Chalut, C. (2016) Trehalose polyphleates are produced by a glycolipid biosynthetic pathway conserved across phylogenetically distant mycobacteria. *Cell Chem. Biol.* **23,** 278–289 CrossRef Medline
6. Seeliger, J., and Moody, D. B. (2016) Monstrous mycobacterial lipids. *Cell Chem. Biol.* **23,** 207–209 CrossRef Medline
7. Llorens-Fons, M., Perez-Trujillo, M., Julian, E., Brambilla, C., Alcaide, F., Byrd, T. F., and Luquin, M. (2017) Trehalose polyphleates, external cell wall lipids in *Mycobacterium abscessus*, are associated with the formation of clumps with cording morphology which have been associated with virulence. *Front. Microbiol.* **8,** 1402 CrossRef Medline
8. Chalut, C. (2016) MmpL transporter-mediated export of cell-wall associated lipids and siderophores in mycobacteria. *Tuberculosis* **100,** 32–45 CrossRef Medline
9. Adindla, S., and Guruprasad, L. (2003) Sequence analysis corresponding to the PPE and PE proteins in *Mycobacterium tuberculosis* and other genomes. *J. Biosci.* **28,** 169–179 CrossRef Medline
10. Sultana, R., Tanneeru, K., and Guruprasad, L. (2011) The PE-PPE domain in mycobacterium reveals a serine α/β hydrolase fold and function: an *in-silico* analysis. *PLoS ONE* **6,** e16745 CrossRef Medline
11. Seeliger, J. C., Holsclaw, C. M., Schelle, M. W., Botyanszki, Z., Gilmore, S. A., Tully, S. E., Niederweis, M., Cravatt, B. F., Leary, J. A., and Bertozzi, C. R. (2012) Elucidation and chemical modulation of sulfolipid-1 biosynthesis in *Mycobacterium tuberculosis*. *J. Biol. Chem.* **287,** 7990–8000 CrossRef Medline
12. Belardinelli, J. M., Larrouy-Maumus, G., Jones, V., Sorio de Carvalho, L. P., McNeil, M. R., and Jackson, M. (2014) Biosynthesis and translocation of unsulfated acyltrehaloses in *Mycobacterium tuberculosis*. *J. Biol. Chem.* **289,** 27952–27965 CrossRef Medline
13. Touchette, M. H., Holsclaw, C. M., Previti, M. L., Solomon, V. C., Leary, J. A., Bertozzi, C. R., and Seeliger, J. C. (2015) The rv1184c locus encodes Chp2, an acyltransferase in *Mycobacterium tuberculosis* polyacyltrehalose lipid biosynthesis. *J. Bacteriol.* **197,** 201–210 CrossRef Medline
14. Auclair, S. M., Bhanu, M. K., and Kendall, D. A. (2012) Signal peptidase I: cleaving the way to mature proteins. *Protein Sci.* **21,** 13–25 CrossRef Medline
15. Wiker, H. G., Wilson, M. A., and Schoolnik, G. K. (2000) Extracytoplasmic proteins of *Mycobacterium tuberculosis*—mature secreted proteins often start with aspartic acid and proline. *Microbiology* **146,** 1525–1533 CrossRef Medline
16. Belardinelli, J. M., and Jackson, M. (2017) Green fluorescent protein as a protein localization and topological reporter in mycobacteria. *Tuberculosis* **105,** 13–17 CrossRef Medline
17. Deshayes, C., Bach, H., Euphrasie, D., Attarian, R., Coureuil, M., Sougakoff, W., Laval, F., Av-Gay, Y., Daffé, M., Etienne, G., and Reyrat, J. M. (2010) MmpS4 promotes glycopeptidolipids biosynthesis and export in *Mycobacterium smegmatis*. *Mol. Microbiol.* **78,** 989–1003 CrossRef Medline
18. Chiaradia, L., Lefebvre, C., Parra, J., Marcoux, J., Burlet-Schiltz, O., Etienne, G., Tropis, M., and Daffé, M. (2017) Dissecting the mycobacterial cell envelope and defining the composition of the native mycomembrane. *Sci. Rep.* **7,** 12807 CrossRef Medline
19. McCann, J. R., McDonough, J. A., Pavelka, M. S., and Braunstein, M. (2007) β-Lactamase can function as a reporter of bacterial protein export during Mycobacterium tuberculosis infection of host cells. *Microbiology* **153,** 3350–3359 CrossRef Medline

20. Palzkill, T., Le, Q. Q., Wong, A., and Botstein, D. (1994) Selection of functional signal peptide cleavage sites from a library of random sequences. *J. Bacteriol.* **176,** 563–568 CrossRef Medline
21. Timm, J., Lim, E. M., and Gicquel, B. (1994) Escherichia coli-mycobacteria shuttle vectors for operon and gene fusions to lacZ: the pJEM series. *J. Bacteriol.* **176,** 6749–6753 CrossRef Medline
22. Fay, A., Czudnochowski, N., Rock, J. M., Johnson, J. R., Krogan, N. J., Rosenberg, O., and Glickman, M. S. (2019) Two accessory proteins govern MmpL3 mycolic acid transport in mycobacteria. *MBio* **10,** e00850-19 CrossRef Medline
23. Touchette, M. H., and Seeliger, J. C. (2017) Transport of outer membrane lipids in mycobacteria. *Biochim. Biophys. Acta* **1862,** 1340–1354 CrossRef Medline
24. Quandt, J., and Hynes, M. F. (1993) Versatile suicide vectors which allow direct selection for gene replacement in Gram-negative bacteria. *Gene* **127,** 15–21 CrossRef Medline
25. Flores, A. R., Parsons, L. M., and Pavelka, M. S., Jr. (2005) Genetic analysis of the β-lactamases of *Mycobacterium tuberculosis* and *Mycobacterium smegmatis* and susceptibility to β-lactam antibiotics. *Microbiology* **151,** 521–532 CrossRef Medline
26. Etienne, G., Malaga, W., Laval, F., Lemassu, A., Guilhot, C., and Daffé, M. (2009) Identification of the polyketide synthase involved in the biosynthesis of the surface-exposed lipooligosaccharides in mycobacteria. *J. Bacteriol.* **191,** 2613–2621 CrossRef Medline
27. Bligh, E. G., and Dyer, W. J. (1959) A rapid method of total lipid extraction and purification. *Can. J. Biochem. Physiol.* **37,** 911–917 CrossRef Medline
28. Perez-Riverol, Y., Csordas, A., Bai, J., Bernal-Llinares, M., Hewapathirana, S., Kundu, D. J., Inuganti, A., Griss, J., Mayer, G., Eisenacher, M., Perez, E., Uszkoreit, J., Pfeuffer, J., Sachsenberg, T., Yilmaz, S., *et al.* (2019) The PRIDE database and related tools and resources in 2019: improving support for quantification data. *Nucleic Acids Res.* **47,** D442–D450 CrossRef Medline
29. Nielsen, H., Engelbrecht, J., Brunak, S., and von Heijne, G. (1997) Identification of prokaryotic and eukaryotic signal peptides and prediction of their cleavage sites. *Protein Eng.* **10,** 1–6 CrossRef Medline
30. Ortalo-Magné, A., Lemassu, A., Lanéelle, M. A., Bardou, F., Silve, G., Gounon, P., Marchal, G., and Daffé, M. (1996) Identification of the surface-exposed lipids on the cell envelopes of Mycobacterium tuberculosis and other mycobacterial species. *J. Bacteriol.* **178,** 456–461 CrossRef Medline
31. Astarie-Dequeker, C., Le Guyader, L., Malaga, W., Seaphanh, F. K., Chalut, C., Lopez, A., and Guilhot, C. (2009) Phthiocerol dimycocerosates of *M. tuberculosis* participate in macrophage invasion by inducing changes in the organization of plasma membrane lipids. *PLoS Pathog.* **5,** e1000289 CrossRef Medline
32. Gutierrez, C., and Devedjian, J. C. (1989) A plasmid facilitating in vitro construction of phoA gene fusions in *Escherichia coli*. *Nucleic Acids Res.* **17,** 3999 CrossRef Medline
33. Le Dantec, C., Winter, N., Gicquel, B., Vincent, V., and Picardeau, M. (2001) Genomic sequence and transcriptional analysis of a 23-kilobase mycobacterial linear plasmid: evidence for horizontal transfer and identification of plasmid maintenance systems. *J. Bacteriol.* **183,** 2157–2164 CrossRef Medline
34. Bouyssié, D., Hesse, A. M., Mouton-Barbosa, E., Rompais, M., Macron, C., Carapito, C., Gonzalez de Peredo, A., Couté, Y., Dupierris, V., Burel, A., Menetrey, J. P., Kalaitzakis, A., Poisat, J., Romdhani, A., Burlet-Schiltz, O., *et al.* (2020) Proline: an efficient and user-friendly software suite for large-scale proteomics. *Bioinformatics* **36,** 3148–3155 CrossRef Medline
35. Gong, C., Bongiorno, P., Martins, A., Stephanou, N. C., Zhu, H., Shuman, S., and Glickman, M. S. (2005) Mechanism of nonhomologous end-joining in mycobacteria: a low-fidelity repair system driven by Ku, ligase D and ligase C. *Nat. Struct. Mol. Biol.* **12,** 304–312 CrossRef Medline
36. Barry, C. E., Crick, D. C., and McNeil, M. R. (2007) Targeting the formation of the cell wall core of *M. tuberculosis*. *Infect. Disord. Drug Targets* **7,** 182–202 CrossRef Medline
37. Li, W., Xin, Y., McNeil, M. R., and Ma, Y. (2006) rmlB and rmlC genes are essential for growth of mycobacteria. *Biochem. Biophys. Res. Commun.* **342,** 170–178 CrossRef Medline
38. Wirth, S. E., Krywy, J. A., Aldridge, B. B., Fortune, S. M., Fernandez-Suarez, M., Gray, T. A., and Derbyshire, K. M. (2012) Polar assembly and scaffolding proteins of the virulence-associated ESX-1 secretory apparatus in mycobacteria. *Mol. Microbiol.* **83,** 654–664 CrossRef Medline
39. Jain, P., and Nagaraja, V. (2005) An atypical type II topoisomerase from *Mycobacterium smegmatis* with positive supercoiling activity. *Mol. Microbiol.* **58,** 1392–1405 CrossRef Medline
40. Plocinski, P., Arora, N., Sarva, K., Blaszczyk, E., Qin, H., Das, N., Plocinska, R., Ziolkiewicz, M., Dziadek, J., Kiran, M., Gorla, P., Cross, T. A., Madiraju, M., and Rajagopalan, M. (2012) *Mycobacterium tuberculosis* CwsA interacts with CrgA and Wag31, and the CrgA-CwsA complex is involved in peptidoglycan synthesis and cell shape determination. *J. Bacteriol.* **194,** 6398–6409 CrossRef Medline
41. Trefzer, C., Škovierová, H., Buroni, S., Bobovská, A., Nenci, S., Molteni, E., Pojer, F., Pasca, M. R., Makarov, V., Cole, S. T., Riccardi, G., Mikušová, K., and Johnsson, K. (2012) Benzothiazinones are suicide inhibitors of mycobacterial decaprenylphosphoryl-β-D-ribofuranose 2'-oxidase DprE1. *J. Am. Chem. Soc.* **134,** 912–915 CrossRef Medline
42. Belanová, M., Dianisková, P., Brennan, P. J., Completo, G. C., Rose, N. L., Lowary, T. L., and Mikusová, K. (2008) Galactosyl transferases in mycobacterial cell wall synthesis. *J. Bacteriol.* **190,** 1141–1145 CrossRef Medline
43. Upadhyay, A., Fontes, F. L., Gonzalez-Juarrero, M., McNeil, M. R., Crans, D. C., Jackson, M., and Crick, D. C. (2015) Partial saturation of menaquinone in *Mycobacterium tuberculosis*: function and essentiality of a novel reductase, MenJ. *ACS Cent. Sci.* **1,** 292–302 CrossRef Medline
44. Schaeffer, M. L., Khoo, K. H., Besra, G. S., Chatterjee, D., Brennan, P. J., Belisle, J. T., and Inamine, J. M. (1999) The pimB gene of *Mycobacterium tuberculosis* encodes a mannosyltransferase involved in lipoarabinomannan biosynthesis. *J. Biol. Chem.* **274,** 31625–31631 CrossRef Medline
45. Palmer, T., and Stansfeld, P. J. (2020) Targeting of proteins to the twin-arginine translocation pathway. *Mol. Microbiol.* **113,** 861–871 CrossRef Medline
46. Fenn, K., Wong, C. T., and Darbari, V. C. (2019) *Mycobacterium tuberculosis* uses Mce proteins to interfere with host cell signaling. *Front. Mol. Biosci.* **6,** 149 CrossRef Medline
47. Hermann, C., Giddey, A. D., Nel, A. J. M., Soares, N. C., and Blackburn, J. M. (2019) Cell wall enrichment unveils proteomic changes in the cell wall during treatment of *Mycobacterium smegmatis* with sub-lethal concentrations of rifampicin. *J. Proteomics* **191,** 166–179 CrossRef Medline
48. Abou-Zeid, C., Smith, I., Grange, J. M., Ratliff, T. L., Steele, J., and Rook, G. A. (1988) The secreted antigens of *Mycobacterium tuberculosis* and their relationship to those recognized by the available antibodies. *J. Gen. Microbiol.* **134,** 531–538 CrossRef Medline
49. Stahl, C., Kubetzko, S., Kaps, I., Seeber, S., Engelhardt, H., and Niederweis, M. (2001) MspA provides the main hydrophilic pathway through the cell wall of *Mycobacterium smegmatis*. *Mol. Microbiol.* **40,** 451–464 CrossRef Medline
50. Simeone, R., Bottai, D., Frigui, W., Majlessi, L., and Brosch, R. (2015) ESX/type VII secretion systems of mycobacteria: insights into evolution, pathogenicity and protection. *Tuberculosis* **95,** S150–S154 CrossRef Medline
51. Roche, P. W., Winter, N., Triccas, J. A., Feng, C. G., and Britton, W. J. (1996) Expression of *Mycobacterium tuberculosis* MPT64 in recombinant *Myco. smegmatis*: purification, immunogenicity and application to skin tests for tuberculosis. *Clin. Exp. Immunol.* **103,** 226–232 CrossRef Medline
52. Ates, L. S. (2020) New insights into the mycobacterial PE and PPE proteins provide a framework for future research. *Mol. Microbiol.* **113,** 4–21 CrossRef Medline
53. Manca, C., Lyashchenko, K., Wiker, H. G., Usai, D., Colangeli, R., and Gennaro, M. L. (1997) Molecular cloning, purification, and serological characterization of MPT63, a novel antigen secreted by *Mycobacterium tuberculosis*. *Infect. Immun.* **65,** 16–23 CrossRef Medline

54. Nagai, S., Wiker, H. G., Harboe, M., and Kinomoto, M. (1991) Isolation and partial characterization of major protein antigens in the culture fluid of *Mycobacterium tuberculosis*. *Infect. Immun.* **59,** 372–382 CrossRef Medline
55. Kocincová, D., Sondén, B., de Mendonça-Lima, L., Gicquel, B., and Reyrat, J. M. (2004) The Erp protein is anchored at the surface by a carboxy-terminal hydrophobic domain and is important for cell-wall structure in *Mycobacterium smegmatis*. *FEMS Microbiol. Lett.* **231,** 191–196 CrossRef Medline
56. Manca, C., Lyashchenko, K., Colangeli, R., and Gennaro, M. L. (1997) MTC28, a novel 28-kilodalton proline-rich secreted antigen specific for the *Mycobacterium tuberculosis* complex. *Infect. Immun.* **65,** 4951–4957 CrossRef Medline
57. Malaga, W., Perez, E., and Guilhot, C. (2003) Production of unmarked mutations in mycobacteria using site-specific recombination. *FEMS Microbiol. Lett.* **219,** 261–268 CrossRef Medline

The final assembly of trehalose polyphleates takes place within the outer layer of the mycobacterial cell envelope

Laurie Thouvenel, Gautier Prevot, Laura Chiaradia, Julien Parra, Emmanuelle Mouton-Barbosa, Marie Locard-Paulet, Julien Marcoux, Maryelle Tropis, Odile Burlet-Schiltz, Mamadou Daffé, Christophe Guilhot, Gilles Etienne and Christian Chalut

J. Biol. Chem. 2020, 295:11184-11194.
doi: 10.1074/jbc.RA120.013299 originally published online June 17, 2020
